The effects of additive elements on the microstructure characteristics and mechanical properties of Cr–Fe–C hard-facing alloys

Chi-Ming Lin, Chia-Ming Chang, Jie-Hao Chen, Weite Wu[*]

National Chung Hsing University, Department of Materials Science and Engineering, 250 Kuo Kuang Road, Taichung 402, Taiwan

ABSTRACT

The present investigation discusses the effects of V, Mo, and Ni addition on the morphologies and mechanical properties of primary carbides and eutectic colonies in Cr–Fe–C hard-facing alloys with hypereutectic compositions. Findings show that V, Mo, and Ni addition obviously affects the hardness and indentation fracture (K_C) of primary carbides and eutectic colonies. V addition to alloy A can slightly increase the hardness of primary carbides varying from 1503 ± 17 to 1551 ± 13 HV but slightly decreases the K_C value of primary carbides ranging from 3.80 ± 0.15 to 3.64 ± 0.14 MPa m$^{1/2}$. Mo addition to alloy B can increase the K_C value of primary carbides ranging from 2.35 ± 0.11 to 2.67 ± 0.08 MPa m$^{1/2}$. Ni addition to alloy B can decrease the hardness of eutectic colonies varying from 769 ± 9 to 608 ± 13 HV. Maximum hardness was obtained in the coated surface of alloy B due to the formation of large amounts of primary M_7C_3 carbides.

© 2010 Elsevier B.V. All rights reserved.

1. Introduction

The high-carbon Cr-based hard-facing alloy is well known for its excellent resistance to abrasion, oxidation, and corrosion, and has been extensively used in aggressive conditions, such as mining and mineral process, cement production, and pulp and paper manufacture industries. Many recent investigations have revealed that the microstructure of Cr–Fe–C hard-facing alloy consists of Cr–Fe solid solution phase (α-ferrite) and complex carbides (such as $M_{23}C_6$ and M_7C_3), depending on the carbon content of hard-facing alloy [1–4].

In the Cr–Fe–C hard-facing alloy, large amounts of primary M_7C_3 carbides uniformly distributed in the $[\alpha + M_7C_3]$ eutectic colonies has the best performances (such as hardness and wear resistance) [4]. M_7C_3 carbides in Cr-based hard-facing alloy are mainly reinforced phases to resist extrinsic substance abrasion and have been widely applied in various composite coatings due to its high hardness and excellent wear resistance [5–10]. Thus, the mechanical properties of primary carbide, such as hardness and K_C, affect both wear and fracture resistance. Accordingly, a detailed knowledge of this hardness and K_C relationship for primary carbide is important to develop high-performance Cr-based hard-facing alloy.

However, few recent studies have focused on the mechanical behavior of primary carbide in Cr–Fe–C hard-facing alloy, due to the experimental difficulties associated with its measurement. Researches readily estimate the fracture toughness in hard materials by inducing cracks at the corners of the indentation, a method known as indentation microfracture (IM) [11–15]. Several authors [11–15] have used the Vickers indentation technique to develop a number of relations between K_C, load (P), indentation diagonal (a), crack length from the center of the indentation (c), elastic modulus (E), Meyer's hardness (H) and Vickers hardness (HV) of a material. Ponton and Rawlings have summarized these relationships [16]. Vickers indentation method has been widely applied in ceramics and hard metals to accurately evaluate the K_C [17–21].

Although much research has been devoted to the microstructure characteristic and the wear resistance in Cr–Fe–C hard-facing alloy, litter research has been done on mechanical properties of primary carbide and eutectic colony. Therefore, the present work is to discuss the effects of additive elements, containing vanadium (V), molybdenum (Mo) and nickel (Ni), on microstructure characteristic of the claddings and mechanical properties of primary carbide and eutectic colony in high-carbon Cr-based hard-facing alloys with hypereutectic compositions. The microstructure evolution of the claddings and the mechanical properties of primary carbide and eutectic colony are systematically characterized by optical microscope (OM), X-ray diffraction (XRD), electron probe microanalyzer (EPMA), Vickers indentation technique, and Rockwell hardness testing (HRC).

2. Experimental procedures

Base metals for the welding surface were prepared from S45C medium carbon steel plates with dimensions of 105 mm × 85 mm × 19 mm. Before welding, these specimens were ground and cleaned with acetone to remove any oxide and grease. To investigate the effects of additive elements (V, Mo, Ni) on the microstructure

* Corresponding author.
E-mail address: wwu@nchu.edu.tw (W. Wu).

Table 1
Alloy filler components.

Filler	Powder ratio (%)				
	Cr	CrC (4:1)	V	Mo	Ni
A	75	25	0	0	0
A + 2V	73	25	2	0	0
B	65	35	0	0	0
B + 6Mo	59	35	0	6	0
B + 6Ni	59	35	0	0	6
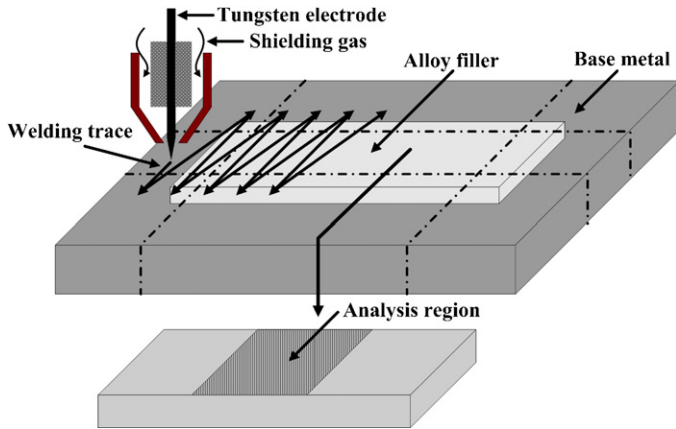
Fig. 1. Schematic illustration of GTAW for hard-facing welding and the analytical region of WDS, XRD, hardness test, and microstructure analysis.

Table 2
Experimental parameters of GTAW surfacing.

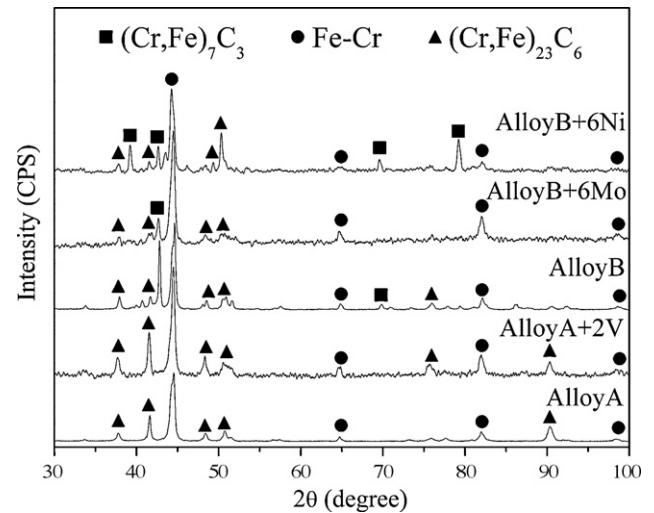| Parameter	Value
Electrode	
Type	W–2%ThO
Diameter	3.2 mm
Angle	30°
Voltage	15 V
Current	220 A
Heat input	6.6 MJ/m
Protective gas	
Type	Ar
Flow	15 L/min
Welding speed	
Travel speed	30 mm/min
Oscillating speed	230 mm/min

Heat input $Q = (60 \times I \times V)/S$, I: current, V: voltage, S: travel speed.

characteristics of high-carbon Cr-based alloys with hypereutectic compositions, the experiment mixed together various Cr, V, Mo, Ni, and CrC (Cr:C = 4:1) powders. Table 1 lists the alloy filler components. The sizes of V and Mo powders are from 30 to 50 μm, 70 to 100 μm for Cr and Ni powders, and 100 to 150 μm for CrC powders. The purity of these alloy powders is 99% at least. Distinct fillers with compact alloy powders were then prepared with a constant high pressure of 105.39 kg cm^{-2}, so as to form alloy fillers with the dimensions of 30 mm × 25 mm × 3 mm.

Bead-on-plate with oscillation were made by an electric power supply using an auto-mechanized system in which the welding torch was moved back and forth at a constant speed above the alloy filler. The gas tungsten arc (GTA) process melted

Fig. 2. XRD patterns of the as-clad Cr-based alloys.

the base metal and the alloy filler to produce the hard-facing alloy. Fig. 1 shows the schematic illustration of GTAW for hard-facing welding and the analytical region of wavelength dispersive X-ray spectrometer (WDS), X-ray diffraction (XRD), hardness test, and microstructure analysis. Table 2 reveals the welding parameter in this work.
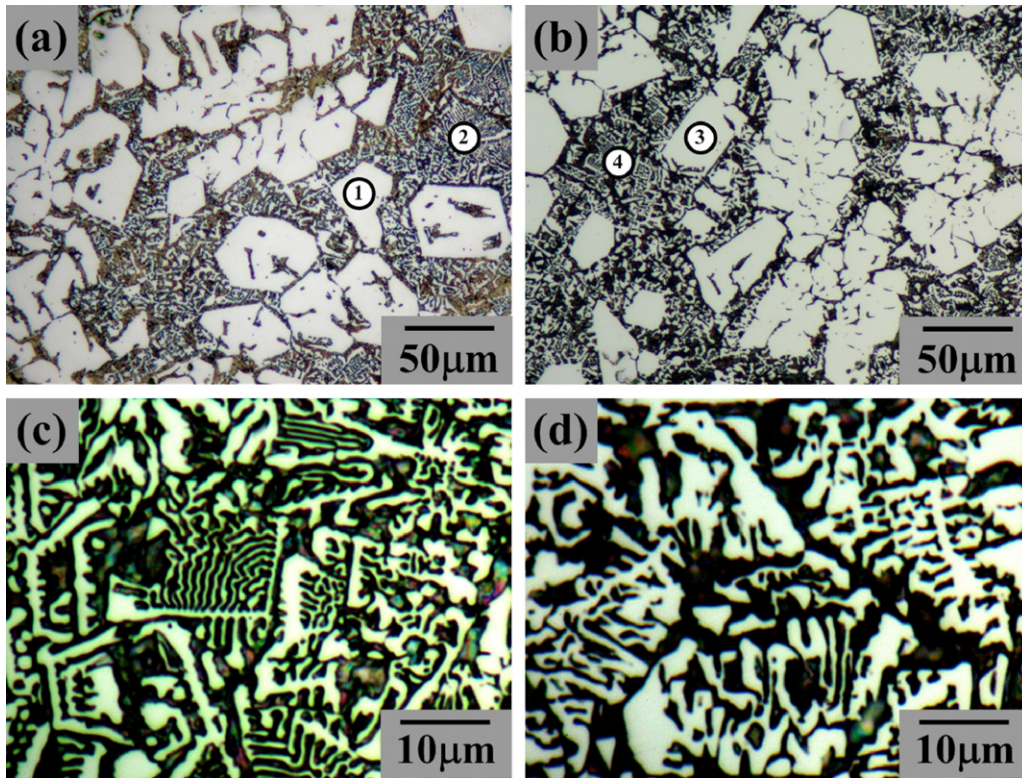
The experiment utilized the WDS to analyze the chemical compositions of hard-facing alloys and the quantitative elemental analysis of constituent phases in microstructure. XRD with Cu Kα radiation was used to identify the constituent phase in the microstructure at a scanning speed of 2 deg/min and 2θ from 30° to 100°. Microstructure characteristic of the claddings was examined by optical microscope (OM). Microstructure investigations were carried out on the top surface, after polishing and etching. The etching agent was composed of 20 g ammonium hydrogen fluoride, 0.5 g potassium pyrosulfite, and 100 ml H_2O at 80 °C.

Hardness of primary phase and eutectic colony was determined by the Vickers hardness tester with a testing load of 0.49 N. The bulk hardness was taken on the top surface of hard-facing alloys by the Rockwell hardness tester (C scale). To form the crack on the indented carbide, the K_C of primary carbide was estimated by the Vickers indentation at 0.98 and 1.96 N. To select the correct equation for calculation K_C, the crack type (radial-median or Palmqvist) was established by a stepwise polishing technique. The evaluation of elastic modulus (E) of primary carbide was measured by nanoindentation with a maximum load of 500 μN. The Palmqvist crack length of indented carbide was measured by field-emission electron scanning microscopy (FE-SEM).

3. Results and discussion

3.1. Phase identification and chemical composition

Fig. 2 shows the phases present in Cr–Fe–C hard-facing alloys produced by the GTAW process. The XRD results indicate that the Fe–Cr solid solution (α) with a b.c.c. structure and the $(Cr,Fe)_{23}C_6$ carbide with a complex f.c.c. structure occurs in alloy A and alloy A + 2V. As well as consisting of an α phase and trace amounts of $(Cr,Fe)_{23}C_6$ carbide, $(Cr,Fe)_7C_3$ carbide with a complex h.c.p. structure exists in alloy B, alloy B + 6Mo, and alloy B + 6Ni. Findings show that adding V, Mo, and Ni into the claddings cannot form new precipitation phases in the microstructure of the claddings.

Table 3
Chemical compositions of the hard-facing alloys.

Alloy	Chemical composition (wt%)									
	C	Fe	Si	Mn	V	Mo	Ni	P	S	Cr
A	3.84	24.5	0.17	0.42	0.00	0.00	0.00	0.004	0.003	Bal.
A + 2V	3.75	20.3	0.14	0.37	1.61	0.00	0.00	0.008	0.004	Bal.
B	5.91	21.1	0.10	0.33	0.00	0.00	0.00	0.011	0.004	Bal.
B + 6Mo	5.79	20.0	0.15	0.65	0.00	5.28	0.00	0.008	0.003	Bal.
B + 6Ni	6.07	20.8	0.17	0.51	0.00	0.00	5.11	0.005	0.003	Bal.

Fig. 3. (a) OM micrograph of alloy A (Cr–24.5Fe–3.84C), (b) OM micrograph of alloy A + 2V (Cr–20.3Fe–3.75C–1.61V), (c) morphologies of the eutectic colonies in alloy A and (d) morphologies of the eutectic colonies in alloy A + 2V.
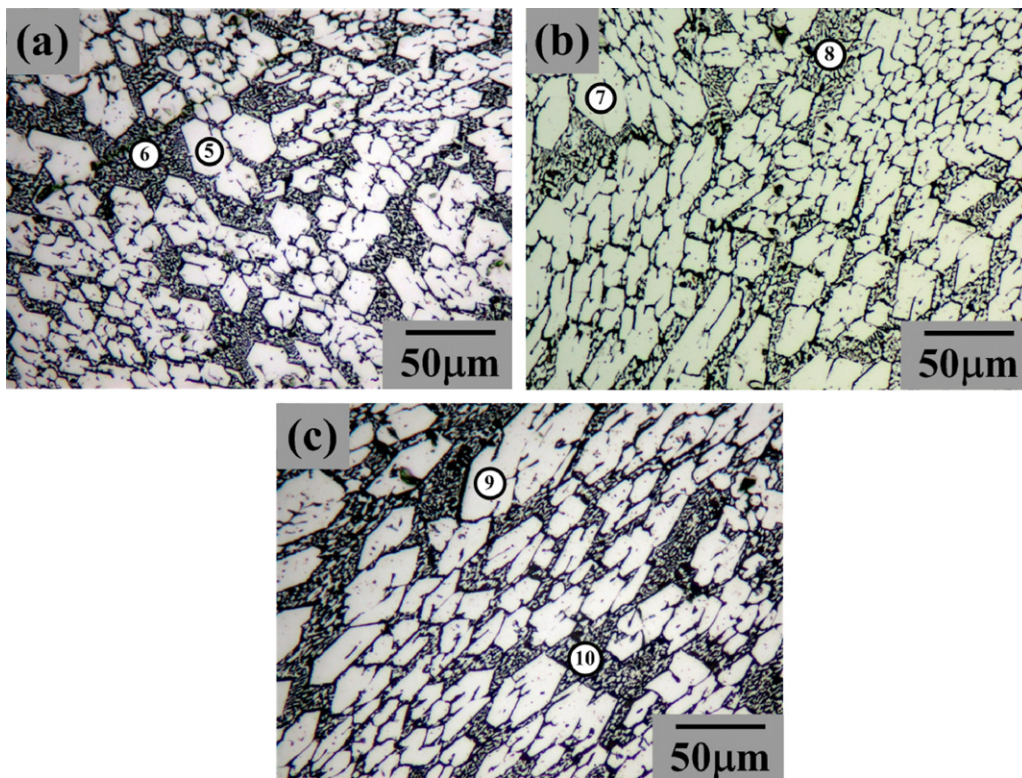
Fig. 4. OM micrographs of high-carbon Cr-based alloy claddings with primary M_7C_3 carbide: (a) alloy B (Cr–21.1Fe–5.91C), (b) alloy B + 6Mo (Cr–20Fe–5.79C–5.28Mo) and (c) alloy B + 6Ni (Cr–20.8Fe–6.07C–5.11Ni).
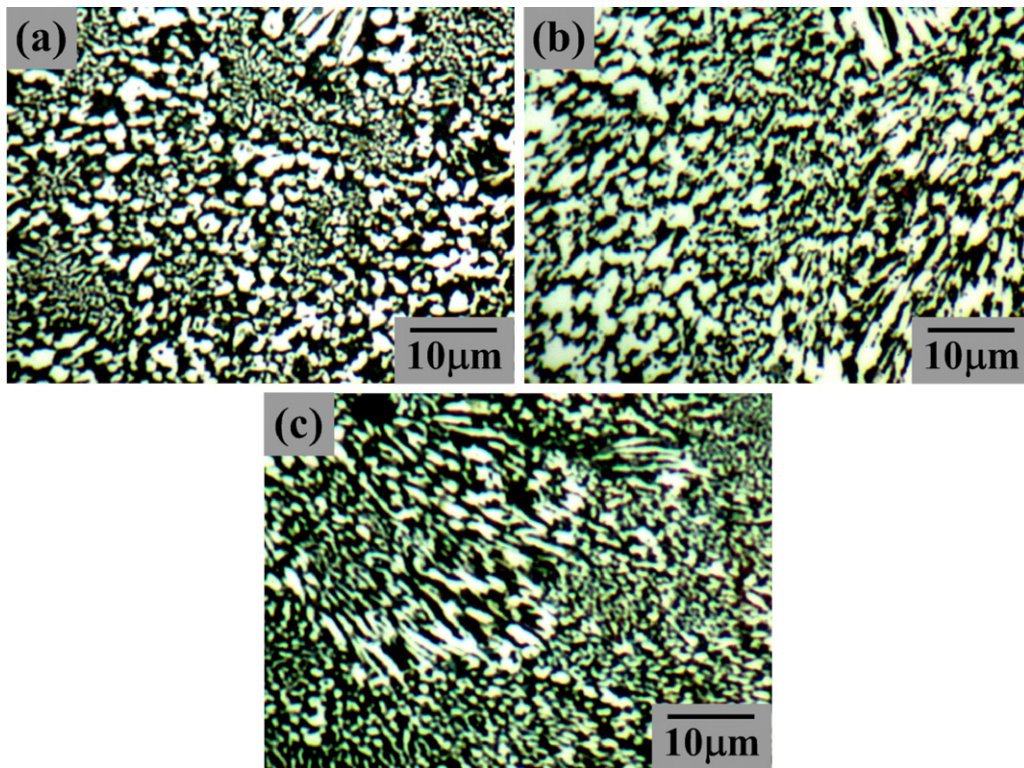
Fig. 5. Morphologies of eutectic colonies in the hard-facing alloys with primary M_7C_3 carbide: (a) alloy B, (b) alloy B + 6Mo and (c) alloy B + 6Ni.

Table 3 lists the chemical compositions of these hard-facing alloys. The analyses are taken from top surfaces of as-clad Cr-based hard-facing alloys. Results show that the C content varies from 3.75 to 6.07 wt%. For alloy A, the hypereutectic structure, carbon content is about 3.84%. For alloy A + 2V, the hypereutectic structure, C and V contents are about 3.75% and 1.61%, respectively. For alloy B, the hypereutectic structure, carbon content is about 5.91%. For alloy B + 6Mo, the hypereutectic structure, C and Mo contents are about 5.79% and 5.28%, respectively. For alloy B + 6Ni, the hypereutectic structure, C and Ni contents are about 6.07% and 5.11%, respectively.

3.2. Surface microstructure observation

Figs. 3–5 reveal the effects of V, Mo, and Ni additions in the alloy filler on the surface microstructure characteristic of as-clad Cr–Fe–C hard-facing alloys. Fig. 3(a) and (b) reveal that the microstructure of alloy A and alloy A + 2V is composed of primary $M_{23}C_6$ carbides and $[\alpha + M_{23}C_6]$ eutectic colonies. The quantitative elemental analysis shown in Table 4 confirms that primary $M_{23}C_6$ carbides in alloy A and alloy A + 2V are $(Cr,Fe)_{23}C_6$ and $(Cr,Fe,V)_{23}C_6$ carbides and their atomic formulae are $Cr_{19.5}Fe_{3.8}C_6$ and $Cr_{19.7}Fe_{3.4}V_{0.4}C_6$, respectively. The morphologies of eutectic $M_{23}C_6$ carbides for alloy A and alloy A + 2V, as presented in Fig. 3(c) and (d), are dendritic in shape. The results in Fig. 3 and Table 4 indicate that adding V to alloy A cannot affect the morphologies of primary carbides and eutectic colonies and can combine with Cr, Fe, and C to form the $(Cr,Fe,V)_{23}C_6$ carbide.

Fig. 4 reveals that primary M_7C_3 carbides form in the surrounding of $[\alpha + M_7C_3]$ eutectic colonies in alloy B, alloy B + 6Mo, and alloy B + 6Ni. The morphologies of eutectic M_7C_3 carbides for alloy B, alloy B + 6Mo, and alloy B + 6Ni, as Fig. 5 shows, are of polygonal shape. The quantitative elemental analysis interpreted in Table 4 confirms that primary M_7C_3 carbides for alloy B, alloy B + 6Mo, and alloy B + 6Ni are $(Cr,Fe)_7C_3$, $(Cr,Fe,Mo)_7C_3$, and $(Cr,Fe)_7C_3$ carbides and their atomic formulae are $Cr_{6.4}Fe_{0.6}C_3$, $Cr_{6.2}Fe_{0.7}Mo_{0.2}C_3$, and $Cr_{6.6}Fe_{0.7}C_3$, respectively. The results in Figs. 4 and 5 and Table 4 indicate that Mo and Ni additions in alloy B cannot affect the morphologies of primary carbides and eutectic colonies. Mo added into alloy B can combine with Cr, Fe, and C to form the $(Cr,Fe,Mo)_7C_6$ carbide. Ni added into alloy B cannot form the $(Cr,Fe,Ni)_7C_6$ carbide and can dissolve into Fe–Cr solid solution to form Fe–Cr–Ni solid solution.

The morphologies of primary $M_{23}C_6$ and M_7C_3 carbides shown in Figs. 3 and 4 are polygonal in shape. The morphological transition

Table 4
Chemical composition of each phase in microstructure by WDS.

| Position	Phase	Cr	Fe	C	Si	Mn	V	Mo	Ni
1	$M_{23}C_6(Cr_{19.5}Fe_{3.8}C_6)$	77.8	16.2	5.53	0.03	0.44	0.00	0.00	0.00
2	$\alpha + M_{23}C_6$	68.1	27.3	3.91	0.15	0.54	0.00	0.00	0.00
3	$M_{23}C_6(Cr_{19.7}Fe_{3.4}V_{0.4}C_6)$	78.0	14.5	5.47	0.04	0.52	1.47	0.00	0.00
4	$\alpha + M_{23}C_6$	70.5	23.6	3.73	0.12	0.36	1.69	0.00	0.00
5	$M_7C_3(Cr_{6.4}Fe_{0.6}C_3)$	81.9	8.85	8.91	0.06	0.28	0.00	0.00	0.00
6	$\alpha + M_7C_3$	70.3	23.8	6.09	0.33	0.52	0.00	0.00	0.00
7	$M_7C_3(Cr_{6.2}Fe_{0.7}Mo_{0.2}C_3)$	77.6	8.95	8.62	0.03	0.37	0.00	3.89	0.00
8	$\alpha + M_7C_3$	63.7	19.1	6.25	0.23	0.32	0.00	10.4	0.00
9	$M_7C_3 (Cr_{6.6}Fe_{0.7}C_3)$	80.6	9.95	8.44	0.06	0.47	0.00	0.00	0.48
10	$\alpha + M_7C_3$	60.8	22.7	6.09	0.33	0.56	0.00	0.00	9.52
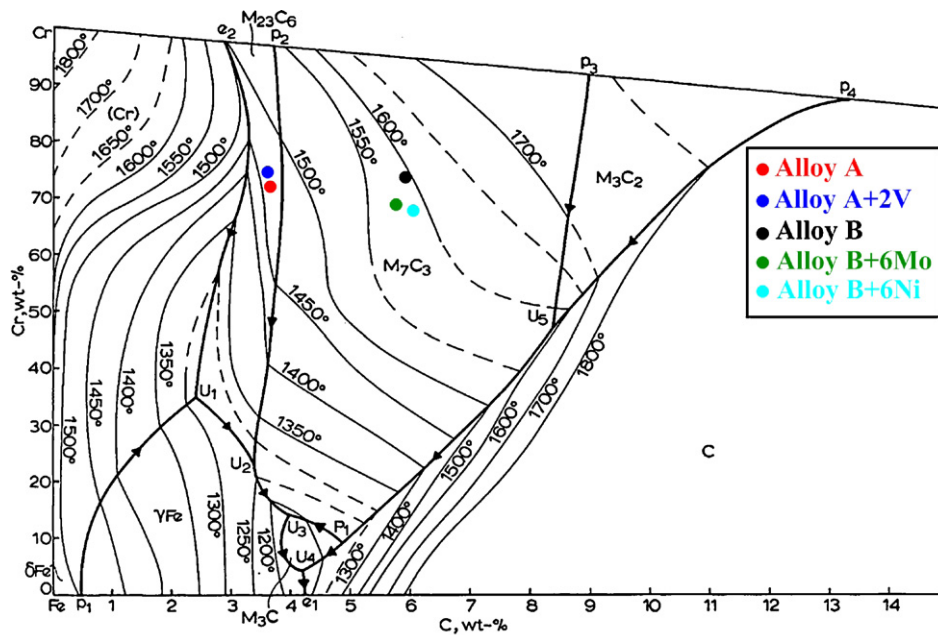
Fig. 6. Liquidus projection for the Fe–Cr–C ternary system.

during the primary phase depends on the type of solid/liquid interface. Melting entropy is a convenient criterion to predict this aspect of crystallization behavior. Values of α ($=\Delta S_f/R$) which are less than 2 imply a tendency to non-faced crystal growth, while higher α-values imply production of faced crystal growth forms [22]. Most intermetallic compounds or minerals have high α-values predicting a faced interface. Hence, primary $M_{23}C_6$ and M_7C_3 carbides have a faced interface. During faced phase solidification, the inherently rough and high-index planes accept added atoms readily and grow quickly. As a result, these planes disappear and the crystal remains, bounded by more slowly growing facets (low-index planes), lead to the formation of a polygonal shape.

Fig. 6 is the liquidus projection of the iron corner of the Fe–Cr–C ternary system [23,24], with five points corresponding to the alloys listed in Table 3. In Fig. 6, with alloy A and alloy A+2V beginning to solidify, $M_{23}C_6$ carbides appear from the melt as primary phases. Then [$\alpha + M_{23}C_6$] eutectic colonies form around the primary phase grain boundary. In alloy B, alloy B+6Mo, and alloy B+6Ni, primary M_7C_3 carbides appear from the melt during the solidification process. When molten poor temperature falls to the eutectic point, the residual melt rejects the Cr and C atoms. Thus, the eutectic colonies [$\alpha + M_7C_3$] subsequently form when the Cr and C concentrations in the residual melt reach the eutectic composition.

3.3. Mechanical properties

Fig. 7 interprets the effects of V, Mo, and Ni on the hardness of primary carbides and eutectic colonies. In Fig. 7(a), the hardness of primary carbides and eutectic colonies in alloy A is lower than in alloy A+2 V. Hence, V added into alloy A raises the hardness of primary carbides and eutectic colonies. In Fig. 7(b), the hardness of primary carbides is alloy B = alloy B+6Ni > alloy B+6Mo and the hardness of eutectic colonies is alloy B+6Mo > alloy B > alloy B+6Ni. Therefore, Mo added into alloy B reduces the hardness of primary carbides and raises the hardness of eutectic colonies. Adding Ni to alloy B lowers the hardness of eutectic colonies.

According to Ref. [25], the hardness of a covalent material is determined by two factors: the number of bonds per unit area and the strength of bonding. Zhang et al. [26] has studied the bonding strength of MC compounds (M = 3d-transition-metal) and shows that the bonding strength of MC is TiC > VC > CrC > MoC > FeC > NiC. V addition in alloy A can combine with Cr, Fe, and C to form the $(Cr,Fe,V)_{23}C_6$ carbide leading to an increase in the hardness for primary carbides and eutectic colonies. Table 4 shows that adding Mo to alloy B can partly dissolve into Fe–Cr solid solution to form Fe–Cr–Mo solid solution leading to a slight increase in the eutectic colony. Additionally Mo can also partly combine with Cr, Fe, and C to form the $(Cr,Fe,Mo)_7C_3$ car-
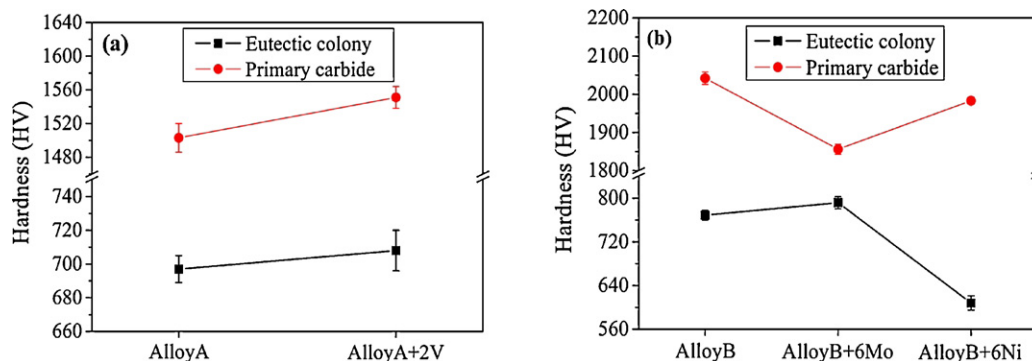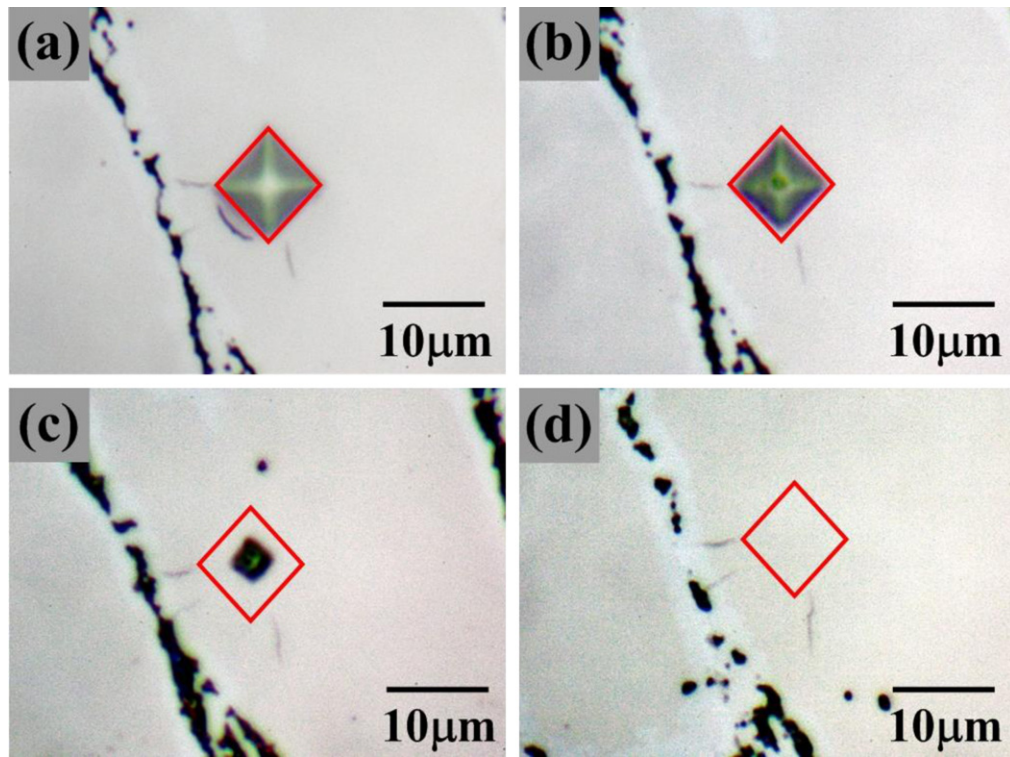

Fig. 7. (a) The effect of the V element on the hardness of each phase in alloy A and (b) the effects of Mo and Ni elements on the hardness of each phase in alloy B.

Fig. 8. Optical graphs of indented M_7C_3 carbide in alloy B after distinct polishing stages: (a) no polishing, (b) polishing for 5 min, (c) polishing for 10 min shows almost complete disappearance of the indentation and (d) polishing for 15 min reveals disappearance of the indentation.

bide. However, the bonding strength of MoC is lower than that of CrC resulting in primary carbide with lower hardness. Dissolving Ni into a Fe–Cr solid solution can soften the matrix, leading to a eutectic colony with lower hardness.

Different formulations exist depending on the cracking systems generated during indentation. When corner cracks are visible at the free surface, they can either be radial-median or Palmqvist cracks. To select an exact K_C equation to estimate the K_C of primary carbide, evaluation cracking systems is very important. The stepwise polishing method is currently used to fully describing cracking systems underneath the indenter [17,20]. A stepwise polishing technique as shown in Fig. 8 reveals that the crack type is Palmqvist. For a Palmqvist cracking system, the following equation is usually employed [12].

$$K_C = 0.0089 \left(\frac{E}{H} \right)^{2/5} \left(\frac{P}{al^{1/2}} \right) \tag{1}$$

where E is Young's modulus (GPa), H is the Vickers hardness (GPa), P is the indentation load (N), a is the half-diagonal of indentation impression (m) and l is the Palmqvist crack length (m).

Fig. 9 shows K_C values of primary carbides evaluated by the Vickers indentation technique using Eq. (1). The result shows a clear difference in the K_C values of primary carbides in Cr–Fe–C hard-facing alloys. These differences are obviously related to their crystalline structure and chemical composition. K_C values of primary M_7C_3 carbides are more than those of primary $M_{23}C_6$ carbides. In $M_{23}C_6$ carbides, adding V to primary carbide can slightly reduce the K_C value range from 3.80 ± 0.15 to 3.64 ± 0.14 MPa m$^{1/2}$ but can slightly increase the hardness value varying from 1503 ± 17 to 1551 ± 13 HV. In M_7C_3 carbides, adding Mo to pri-
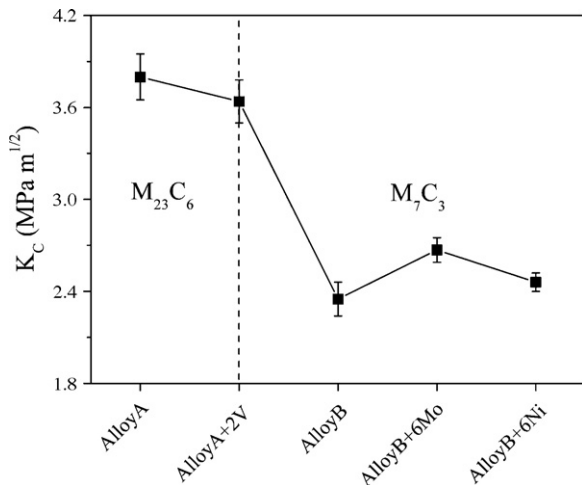
Fig. 9. Effects of V, Mo, and Ni on the K_C of various primary carbides.
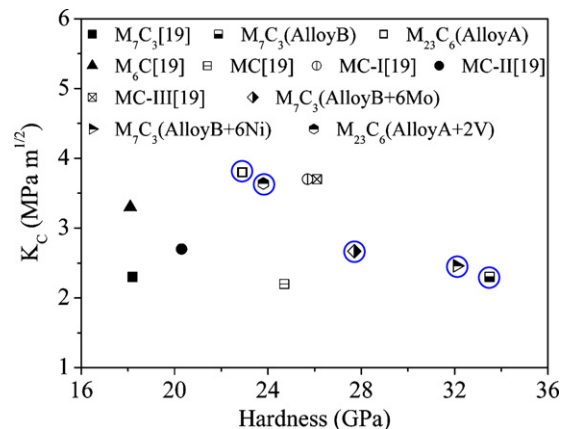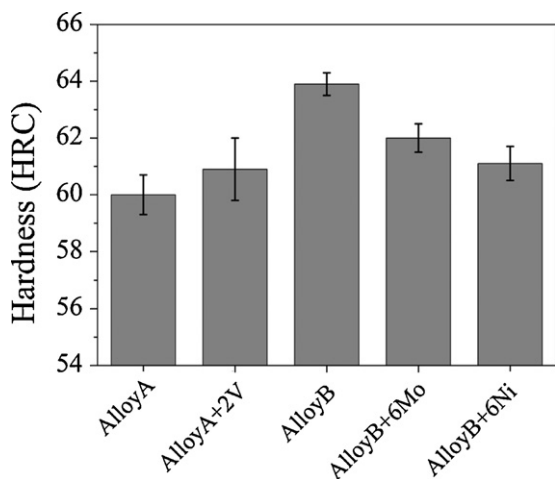

Fig. 10. Hardness and K_C of different carbides.

Fig. 11. Hardness of the as-clad Cr-based alloys.

mary carbide can raise the K_C value range from 2.35 ± 0.11 to 2.67 ± 0.08 MPa m$^{1/2}$.

Casellas et al. [19] evaluated the K_C of carbides with chromium, vanadium, and wolfram in tool steels by a nanoindentation method using the Laugier equation. Reported values for this work [19] are shown in Fig. 10, together with the experimental values obtained in the present work. The result shows that M$_7$C$_3$ carbides in alloy B and alloy B + 6Ni have excellent hardness but poor K_C in all conditions. Inversely, M$_{23}$C$_6$ carbide in alloy A has an excellent K_C but poor hardness in all conditions. V and Mo additions to Cr–Fe–C hard-facing alloys can transform the mechanical properties of primary carbides and eutectic colonies and develop high-performance Cr–Fe–C hard-facing alloys.

Fig. 11 shows the hardness of as-clad Cr–Fe–C hard-facing alloys. The result indicates that maximum hardness is obtained in the coated surface of alloy B due to the formation of large amounts of primary M$_7$C$_3$ carbides. The Vickers hardness of primary M$_7$C$_3$ carbides in the present work is about 1900 HV, 1.3 times greater than that of primary M$_{23}$C$_6$ carbides in the present work, as Fig. 7 shows V added into alloy A can increase the hardness of primary carbides and eutectic colonies leading to cladding with greater hardness. Mo and Ni additions to alloy B can decrease the hardness of primary carbides or eutectic colonies resulting in claddings with less hardness.

4. Conclusion

The purpose of this work is to discuss the effects of V, Mo, and Ni addition on the morphologies and mechanical properties of primary carbides and eutectic colonies in Cr–Fe–C hard-facing alloys with hypereutectic compositions. Results show that V, Mo, and Ni

addition in the investigated quantities cannot affect the morphologies of primary carbides and eutectic colonies. Nevertheless, V, Mo, and Ni addition transforms the mechanical properties of primary carbides and eutectic colonies and develops high-performance Cr–Fe–C hard-facing alloys. V affects slightly the mechanical properties of primary carbide in alloy A due to its trace addition. V addition to alloy A can slightly increase the hardness of primary carbides varying from 1503 ± 17 to 1551 ± 13 HV but slightly reduce the K_C value of primary carbide. Mo addition to alloy B can increase the K_C value of primary carbide varying from 2.35 ± 0.11 to 2.67 ± 0.08 MPa m$^{1/2}$. Maximum hardness was found in the coated surface of alloy B due to the formation of large amounts of primary M$_7$C$_3$ carbides.

References

[1] S.O. Yılmaz, Surf. Coat. Technol. 201 (2006) 1568–1575.
[2] C. Fan, M.C. Chen, C.M. Chang, W. Wu, Surf. Coat. Technol. 201 (2006) 908–912.
[3] C.W. Kuo, C. Fan, S.H. Wu, W. Wu, Mater. Trans. 48 (2007) 2324–2328.
[4] C.M. Lin, C.M. Chang, J.H. Chen, C.C. Hsieh, W. Wu, Metall. Mater. Trans. A 40 (2009) 1031–1038.
[5] J.B. Cheng, B.S. Xu, X.B. Liang, Y.X. Wu, Mater. Sci. Eng. A 492 (2008) 407–412.
[6] V.E. Buchanan, P.H. Shipway, D.G. McCartney, Wear 263 (2007) 99–110.
[7] Y.F. Liu, J.M. Han, R.H. Li, W.J. Li, X.Y. Xu, J.H. Wang, S.Z. Yang, Appl. Surf. Sci. 252 (2006) 7539–7544.
[8] Y.F. Liu, Z.Y. Xia, J.M. Han, G.L. Zhang, S.Z. Yang, Surf. Coat. Technol. 201 (2006) 863–867.
[9] H. Berns, Wear 254 (2003) 47–54.
[10] J.D. Xing, Y.M. Gao, E.Z. Wang, C.G. Bao, Wear 252 (2002) 755–760.
[11] G.R. Anstis, P. Chantikul, B.R. Lawn, D.B. Marshall, J. Am. Ceram. Soc. 64 (1981) 533–538.
[12] K. Niihara, R. Morena, D.P.H. Hasselman, J. Mater. Sci. Lett. 1 (1982) 13–16.
[13] M.T. Laugier, J. Mater. Sci. Lett. 4 (1985) 1539–1541.
[14] D.K. Shetty, I.G. Wright, P.N. Mincer, A.H. Clauer, J. Mater. Sci. 20 (1985) 1873–1882.
[15] M.T. Laugier, J. Mater. Sci. Lett. 6 (1987) 355–356.
[16] C.B. Ponton, R.D. Rawlings, Mater. Sci. Technol. 5 (1989) 865–872.
[17] V. Keryvin, V.H. Hoang, J. Shen, Intermetallics 17 (2009) 211–217.
[18] H. Miyazaki, H. Hyuga, Y. Yoshizawa, K. Hirao, T. Ohji, J. Eur. Ceram. Soc. 29 (2009) 1535–1542.
[19] D. Casellas, J. Caro, S. Molas, J.M. Prado, I. Valls, Acta Mater. 55 (2007) 4277–4286.
[20] V. Milekhine, M.I. Onsoien, J.K. Solberg, T. Skaland, Intermetallics 10 (2002) 743–750.
[21] D. Casellas, I. Rafols, L. Llanes, M. Anglada, Int. J. Refract. Met. H. 17 (1999) 11–20.
[22] W. Kurz, D.J. Fisher, Fundamentals of Solidification, Trans Tech Publications, Switzerland, 1984.
[23] G.V. Raynor, V.G. Rivlin, Phase Equilibria in Iron Ternary Alloys, The Institute of Metals, The Bath Press, UK, 1988.
[24] R.S. Jackson, J. Iron Steel Inst. 208 (1970) 163–167.
[25] F. Gao, Phys. Rev. B 73 (2006) 132104.
[26] Y. Zhang, J. Li, L. Zhou, S. Xiang, Solid State Commun. 121 (2002) 411–416.